Continuum Mech. Thermodyn. (2020) 32:369–385
https://doi.org/10.1007/s00161-018-0728-5

ORIGINAL ARTICLE

Bruno Musil · **Michael Johlitz** · **Alexander Lion**

On the ageing behaviour of NBR: chemomechanical experiments, modelling and simulation of tension set

Received: 16 July 2018 / Accepted: 26 October 2018 / Published online: 31 October 2018

Abstract Rubber components produced from nitrile butadiene rubber (NBR) are changing their material properties due to environmental influences. This is caused by irreversible changes occurring in the elastomer network which is known as chemical ageing. In this paper, ageing behaviour of NBR is investigated and modelled under the influence of different surrounding media as air and oil. Based on the previous works, in which chemical ageing was also modelled, a continuum mechanical approach is introduced here, whereby the rubber viscoelasticity is taken into account. Simulations using FEM are then carried out under different chemical and mechanical boundary conditions, and the proposed modelling approach is validated by means of tension set measurements.

Keywords Chemical ageing · NBR · Viscoelasticity · Tension set

1 Introduction

Elastomers are used in almost all areas of the industrial applications, such as engine mounts, bridge bearings, seals or coatings. During their use in operation, they are exposed to different environmental influences, which lead to the chemical ageing and ultimately to a degradation of the mechanical properties [8]. These include in particular climatic factors such as oxygen, temperature, light (UV radiation) and the influence of media (e.g. oils, fuels). In this work, nitrile butadiene rubber (NBR) is investigated under the influence of different media such as air and oil. Because of its resistance to non-polar liquids, NBR is used in many areas of automotive engineering.

Chemical ageing of elastomers has been already investigated in several studies by different experimental (chemical and mechanical) methods (see, for example [1,4,5,23,31]). As it is widely known, chemical ageing of elastomers results in irreversible changes in the internal structure of the network. Influences of external media lead to scission of the primary network of elastomer and thus to its degradation. In parallel, there is a creation of new network junctions, which is often called network reformation [3,26,29]. It has been also experimentally demonstrated that chemical ageing processes are hardly influenced by mechanical deformations of up to 200% [17,29].

The continuum mechanical modelling approach of ageing is based on modifications in the elastomer network. An internal variable q_d represents the network degradation, and q_r represents the network reformation. Therefore, both parameters are equal to zero for the initial state and equal one for the completely aged state. This type of modelling was proposed in the work by Johlitz [21], and Lion and Johlitz [13] and later also presented in the work of [14] as based on the finite strain theory.

Communicated by Johlitz, Laiarinandrasana and Marco.

B. Musil (✉) · M. Johlitz · A. Lion
Institute of Mechanics, Universität der Bundeswehr München, Werner-Heisenberg-Weg 39, 85579 Neubiberg, Germany
E-mail: bruno.musil@unibw.de

Table 1 Components of the NBR mixture

Component	Amount (phr)
NBR 1846	100
Filler (carbon black N 550)	60
Plasticizer (DEHP)	20
Antioxidant (6-PPD)	2
Zinc oxide	5
Stearic acid	1
Sulphur	2
CBS	1.5
TMTM-80	0.5

In the current work, the modelling concept is extended to finite viscoelasticity. This is especially important when we talk about carbon black filled elastomers such as NBR. The relaxation properties are thus not negligible and can represent up to 20% of the stress drop in a sealing ring measured by the chemical stress relaxation. The modelling concept in this work is based on the concept proposed by Johlitz et al. [15] to model dissipative heating of elastomers. In that work, the viscoelasticity was considered and a thermo-mechanical coupling was created. Thus, in this paper, the concept of [15] is modified and extended by ageing effects. Finally, mechanical behaviour under uniaxial tension and the tension set behaviour of NBR is simulated within this modelling approach and validated by measured data. The motivation for modelling tension or compression set is the possibility to simulate this complex ageing phenomenon and so be able to predict when a rubber component or a seal is no longer suitable for operation.

Nitrile butadiene rubber was prepared according to the formulation shown in Table 1. The oil used for the storage was the standardized reference oil IRM 901 according to the german norm DIN ISO 1817, which is representative for mineral oils with low content of additives.

2 Theory

From the perspective of the kinematics, we consider a multiplicative split of the deformation gradient tensor $\mathbf{F}$ (see [9,18,19,22] or [25]). First, a split of the deformation gradient into volumetric $\bar{\mathbf{F}}$ and isochoric $\hat{\mathbf{F}}$ part is introduced

$$\mathbf{F} = \hat{\mathbf{F}} \cdot \bar{\mathbf{F}}. \tag{1}$$

Thus, an isochoric–volumetric intermediate configuration (IVIC) is motivated. It is assumed that the material behaves nearly mechanically incompressible, which is ensured by the choice of the compression modulus K to be three orders of magnitude higher than the shear modulus. In order to consider the mentioned viscoelasticity of NBR, a further split of the isochoric deformation gradient into the isochoric elastic part $\hat{\mathbf{F}}_\mathrm{e}$ and the isochoric inelastic part $\hat{\mathbf{F}}_\mathrm{i}$ motivates an elastic–inelastic intermediate configuration (EIIC)

$$\hat{\mathbf{F}} = \hat{\mathbf{F}}_\mathrm{e} \cdot \hat{\mathbf{F}}_\mathrm{i}. \tag{2}$$

Furthermore, the following strain measures operating on the reference configuration (RC) are obtained

$$\begin{aligned} \mathbf{C} &= \mathbf{F}^T \cdot \mathbf{F} \\ \mathbf{E} &= \frac{1}{2}\left(\mathbf{C} - \mathbf{I}\right), \end{aligned} \tag{3}$$

where $\mathbf{C}$ is the right Cauchy–Green deformation tensor and $\mathbf{E}$ the Green strain tensor. Using a volumetric push forward operation of $\mathbf{E}$, we obtain a strain tensor $\boldsymbol{\Gamma}$ on the IVIC

$$\boldsymbol{\Gamma} = \frac{1}{2}\left(\hat{\mathbf{C}} - \mathbf{I}\right) + \frac{1}{2}\left(\mathbf{I} - \bar{\mathbf{B}}^{-1}\right) = \hat{\boldsymbol{\Gamma}} + \bar{\boldsymbol{\Gamma}}, \tag{4}$$

with

$$\begin{aligned} \hat{\mathbf{C}} &= \hat{\mathbf{F}}^T \cdot \hat{\mathbf{F}} = J^{-\frac{2}{3}}\,\mathbf{C} \\ \bar{\mathbf{B}} &= \bar{\mathbf{F}} \cdot \bar{\mathbf{F}}^T = J^{\frac{2}{3}}\,\mathbf{I} \\ J &= \det \mathbf{F}. \end{aligned} \tag{5}$$

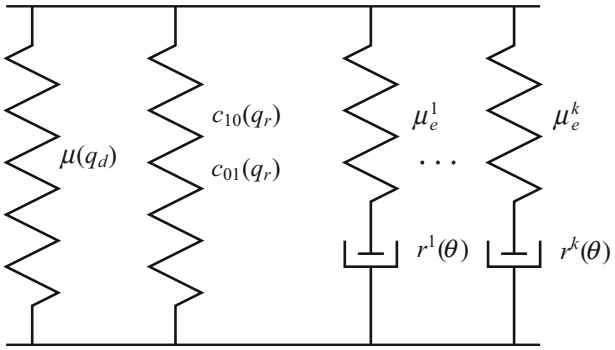

Fig. 1 Rheological model for description of viscoelastic and ageing behaviour

Regarding the thermo-mechanical consistent formulation of the material model, the second law of thermodynamics in the form of Clausius–Duhem inequality is used

$$-\rho_0\,\dot{\psi} + \mathbf{S} : \dot{\mathbf{E}} - \rho_0\, s\,\dot{\theta} - \frac{\mathbf{Q}}{\theta} \cdot \operatorname{Grad}\theta \geq 0, \tag{6}$$

with the second Piola–Kirchhoff stress tensor $\mathbf{S}$, the specific entropy s, the Helmholtz free energy density ψ, the heat flux vector $\mathbf{Q}$ and the density ρ_0. According to the work of [15,20], the stress power $\mathbf{S} : \dot{\mathbf{E}}$ can be rewritten as

$$\mathbf{S} : \dot{\mathbf{E}} = -p\,\dot{J} + J\,\hat{\mathbf{S}} : \dot{\hat{\mathbf{\Gamma}}}, \tag{7}$$

which will be essential for the formulation of the material model. In this equation, p is assumed to be a function of the volume change J and the temperature θ. In analogy to [15], the stress tensor $\hat{\mathbf{S}}$ acting on the IVIC is introduced. In general, $\hat{\mathbf{S}}$ can be obtained from the deviatoric part of the Cauchy stress tensor $\mathbf{T}^{\mathrm{D}}$

$$\hat{\mathbf{S}} = \hat{J}\,\hat{\mathbf{F}}^{-1} \cdot \mathbf{T}^{\mathrm{D}} \cdot \hat{\mathbf{F}}^{-T} = \hat{\mathbf{F}}^{-1} \cdot \mathbf{T}^{\mathrm{D}} \cdot \hat{\mathbf{F}}^{-T}, \tag{8}$$

whereby the variable $\hat{J} = \det\hat{\mathbf{F}} = 1$.

The material model, which is supposed to represent both the viscoelastic and the ageing behaviours, is motivated by a simple rheological model (Fig. 1). A model for small strains can be found at [13] or [16]. Two parallel springs, which represent the equilibrium stress, are connected in parallel with Maxwell elements. The Maxwell elements represent the temperature-dependent viscoelasticity. It is assumed that ageing only influences on the equilibrium stress, which also coincides with the experimental research of [29]. However, an extension of the influence of ageing on the Maxwell elements would be possible. The first spring of basic elasticity represents the degrading network (primary network). The second spring represents the reforming network (secondary network), which builds up stress-free under constant strain. For this purpose, a hypoelastic formulation of the constitutive equation is used, with the corresponding Helmholtz free energy function in the form of history functional Eq. $(9)_3$. A similar model was used in the work of [12,21]. From all these considerations, an additive split of the specific Helmholtz free energy ψ is motivated

$$\begin{aligned}
\psi &= \psi_{\mathrm{eq}}^{\mathrm{vol}}(J,\theta) + \psi_{\mathrm{eq}}^{\mathrm{iso}}\left(\hat{\mathbf{C}}, q_{\mathrm{d}}, q_{\mathrm{r}}\right) + \sum_{k=1}^{m} \psi_{\mathrm{neq}}^{k}\left(\hat{\mathbf{C}}_{\mathrm{e}}^{k}\right) \\
\psi_{\mathrm{eq}}^{\mathrm{iso}} &= \psi_{\mathrm{d}}(\hat{\mathbf{C}}, q_{\mathrm{d}}) + \psi_{\mathrm{r}} \\
\psi_{\mathrm{r}} &= \frac{1}{2}\int_0^t \left(\left[\overset{4}{\mathbf{D}}_{\mathrm{IV}}(s)\; q_{\mathrm{r}}(s)\right]' : \left[\hat{\mathbf{\Gamma}}(t) - \hat{\mathbf{\Gamma}}(s)\right]\right) : \left[\hat{\mathbf{\Gamma}}(t) - \hat{\mathbf{\Gamma}}(s)\right] \mathrm{d}s.
\end{aligned} \tag{9}$$

The time derivative of ψ results to

$$\begin{aligned}
\dot{\psi} = {} & \frac{\partial \psi_{\mathrm{eq}}^{\mathrm{vol}}}{\partial J}\,\dot{J} + \frac{\partial \psi_{\mathrm{eq}}^{\mathrm{vol}}}{\partial \theta}\,\dot{\theta} + \frac{\partial \psi_{\mathrm{d}}}{\partial \hat{\mathbf{C}}} : \dot{\hat{\mathbf{C}}} + \frac{\partial \psi_{\mathrm{d}}}{\partial q_{\mathrm{d}}} : \dot{q}_{\mathrm{d}} \\
& + \left(\frac{1}{2}\int_0^t \left[\overset{4}{\mathbf{D}}_{\mathrm{IV}}(s)\; q_{\mathrm{r}}(s)\right]' : \left[\hat{\mathbf{\Gamma}}(t) - \hat{\mathbf{\Gamma}}(s)\right] \mathrm{d}s\right) : \dot{\hat{\mathbf{C}}} + \frac{\partial \psi_{\mathrm{neq}}}{\partial \hat{\mathbf{C}}_{\mathrm{e}}} : \dot{\hat{\mathbf{C}}}_{\mathrm{e}},
\end{aligned} \tag{10}$$

with

$$\dot{\hat{\mathbf{C}}}_{\mathrm{e}} = \hat{\mathbf{F}}_{\mathrm{i}}^{-T} \cdot \dot{\hat{\mathbf{C}}} \cdot \hat{\mathbf{F}}_{\mathrm{i}}^{-1} - \hat{\mathbf{L}}_{\mathrm{i}}^{T} \cdot \hat{\mathbf{C}}_{\mathrm{e}} - \hat{\mathbf{C}}_{\mathrm{e}} \cdot \hat{\mathbf{L}}_{\mathrm{i}}. \tag{11}$$

Using the relation $\dot{\hat{\mathbf{\Gamma}}} = \frac{1}{2}\dot{\hat{\mathbf{C}}}$ and taking also Eq. (7) into account, the second law of thermodynamics (Eq. 6) can be reformulated as follows

$$\begin{aligned} &- \left(\rho_0\, s + \rho_0 \frac{\partial \psi_\theta}{\partial \theta}\right) \dot{\theta} - \left(p + \rho_0 \frac{\partial \psi_{\mathrm{eq}}^{\mathrm{vol}}}{\partial J}\right) \dot{J} - \frac{\mathbf{Q}}{\theta} \cdot \operatorname{Grad} \theta \\ &+ \left(\frac{1}{2}\, J\, \hat{\mathbf{S}} - \rho_0 \frac{\partial \psi_{\mathrm{d}}}{\partial \hat{\mathbf{C}}} - \frac{1}{2}\, \hat{\mathbf{S}}_{\mathrm{r}} - \rho_0\, \hat{\mathbf{F}}_{\mathrm{i}}^{-1} \cdot \frac{\partial \psi_{\mathrm{neq}}^{\mathrm{iso}}}{\partial \hat{\mathbf{C}}_{\mathrm{e}}} \cdot \hat{\mathbf{F}}_{\mathrm{i}}^{-T}\right) : \dot{\hat{\mathbf{C}}} \\ &+ \frac{\partial \psi_{\mathrm{d}}}{\partial q_{\mathrm{d}}}\, \dot{q}_{\mathrm{d}} + \rho_0 \sum_k \frac{\partial \psi_{\mathrm{neq}}^{k}}{\partial \hat{\mathbf{C}}_{\mathrm{e}}} : \left(\hat{\mathbf{C}}_{\mathrm{e}}^{k} \cdot \hat{\mathbf{L}}_{\mathrm{i}} + \hat{\mathbf{L}}_{\mathrm{i}}^{T} \cdot \hat{\mathbf{C}}_{\mathrm{e}}^{k}\right) \geq 0. \end{aligned} \tag{12}$$

Thus, keeping the $\frac{1}{2}\, \hat{J}\, \hat{\mathbf{C}}^{-1} : \dot{\hat{\mathbf{C}}} = 0$ incompressibility constraint in mind and based on the argumentation of [6] inequality (12) can be evaluated to the following constitutive relationships:

$$\begin{aligned} p &= -\rho_0 \frac{\partial \psi_{\mathrm{eq}}^{\mathrm{vol}}}{\partial J} \\ \rho_0\, s &= -\rho_0 \frac{\partial \psi_{\mathrm{eq}}^{\mathrm{vol}}}{\partial \theta} \\ \mathbf{Q} &= -\lambda_\theta \operatorname{Grad} \theta \\ J\, \hat{\mathbf{S}} &= 2\left[\rho_0 \frac{\partial \psi_{\mathrm{d}}}{\partial \hat{\mathbf{C}}} + \rho_0\, \frac{1}{2}\, \hat{\mathbf{S}}_{\mathrm{r}} + \rho_0\, \hat{\mathbf{F}}_{\mathrm{i}}^{-1} \cdot \frac{\partial \psi_{\mathrm{neq}}}{\partial \hat{\mathbf{C}}_{\mathrm{e}}} \cdot \hat{\mathbf{F}}_{\mathrm{i}}^{-T}\right] + \Phi\, \hat{\mathbf{C}}^{-1}, \end{aligned} \tag{13}$$

with

$$\hat{\mathbf{S}}_{\mathrm{r}} = \int_0^t [\overset{4}{\mathbf{D}}_{\mathrm{IV}}\, (s)\; q_{\mathrm{r}}(s)]' : [\hat{\mathbf{\Gamma}}(t) - \hat{\mathbf{\Gamma}}(s)]\, \mathrm{d}s. \tag{14}$$

To describe the heat flux vector $\mathbf{Q}$, the Fourier's law of heat conduction is applied, with the coefficient of thermal conductivity λ_θ. Thus, it is ensured that the term with $\mathbf{Q}$ always satisfies the Clausius–Duhem inequality (Eq. 6). For the isochoric strain tensor $\hat{\mathbf{C}}$, only its five components can be selected freely and its sixth component follows from the incompressibility constraint. Therefore, similar to the work of [15], the therm $\Phi\, \hat{\mathbf{C}}^{-1}$ is introduced. The function Φ must be determined so that the stress tensor $\hat{\mathbf{S}}$ will have a deviatoric form after transporting it to the actual configuration using Eq. (8). Then, the calculation of the expression $\operatorname{tr} \mathbf{T}^{\mathrm{D}} = \mathbf{I} : \mathbf{T}^{\mathrm{D}} = 0$ will lead to the function Φ

$$\Phi = -\frac{2}{3}\left(\frac{\partial \psi_{\mathrm{d}}}{\partial \hat{\mathbf{C}}} : \hat{\mathbf{C}} + \frac{1}{2}\, \hat{\mathbf{S}}_{\mathrm{r}} : \hat{\mathbf{C}} + \frac{\partial \psi_{\mathrm{neq}}^{k}}{\partial \hat{\mathbf{C}}_{\mathrm{e}}} : \hat{\mathbf{C}}_{\mathrm{e}}^{k}\right). \tag{15}$$

Finally, the dissipation inequality is still to be evaluated. The first part related to ψ_{neq} is evaluated similarly to [15], so that a thermo-mechanical consistent evolution equation for the inelastic isochoric right Cauchy–Green tensor $\hat{\mathbf{C}}_{\mathrm{i}}$ can be formulated. For the specific Helmholtz free energy of the springs of the Maxwell elements, a Neo-Hookean approach is used

$$\rho_0\, \psi_{\mathrm{neq}}^{k}(\hat{\mathbf{C}}_{\mathrm{e}}) = \frac{1}{2}\, \mu_e^{k}\left(\mathrm{I}_{\hat{\mathbf{C}}_{\mathrm{e}}} - 3\right). \tag{16}$$

Hence, the evolution equations

$$\dot{\hat{\mathbf{C}}}_{\mathrm{i}}^{k} = \frac{2}{r^k(\theta)}\left(\hat{\mathbf{C}} - \frac{1}{3} \operatorname{tr}\left(\hat{\mathbf{C}} \cdot (\hat{\mathbf{C}}_{\mathrm{i}}^{k})^{-1}\right) \hat{\mathbf{C}}_{\mathrm{i}}^{k}\right) \tag{17}$$

are compatible with a non-negative rate of dissipation. The second part of the dissipation inequality with respect to ψ_{d} is treated similar to [21] or [14]. This results in some conditions for the dependence of the material parameter μ of the primary network on the internal variable q_{d}

$$\mu(q_{\mathrm{d}}) = \mu_0\, (1 - q_{\mathrm{d}}). \tag{18}$$

For this purpose, an evolution equation for the internal variable q_d of the network degradation is needed, which takes into account the temperature dependence of the process

$$\dot{q_\mathrm{d}} = \nu_\mathrm{d}\, e^{-\frac{E_\mathrm{d}}{R\theta}}(1 - q_\mathrm{d}), \quad q_\mathrm{d}(0) = 0. \tag{19}$$

In the same sense, an evolution equation for the internal variable q_r of the network reformation is formulated

$$\dot{q_\mathrm{r}} = \nu_\mathrm{r}\, e^{-\frac{E_\mathrm{r}}{R\theta}}(1 - q_\mathrm{r}), \quad q_\mathrm{r}(0) = 0, \tag{20}$$

which is also dependent on the temperature θ. In Eqs. (19) and (20), R represents the universal gas constant and the parameters ν_d, ν_r and E_d, E_r are pre-exponential factors and activation energies. The two evolution equations are based on the experimental observations, since both network processes exhibit Arrhenius-like behaviour. Furthermore, in order to describe inhomogeneous ageing processes, the two established evolution equation should be formulated in a different way, e.g. $\dot{q_\mathrm{d}} = f(c, \theta, q_\mathrm{d}, q_\mathrm{r}, \ldots)$, $\dot{q_\mathrm{r}} = f(c, \theta, q_\mathrm{d}, q_\mathrm{r}, \ldots)$, whereby the ageing processes could be coupled and dependent on the local oxygen concentration c, like proposed in [16]. According to this, further investigations are necessary.

3 Experiments and modelling

3.1 Ageing model

As mentioned in the previous chapter (Sect. 1), two dominant processes take place in the elastomer network during ageing: chain scission (network degradation) and the creation of new network junctions (network reformation). In order to study these processes experimentally (phenomenologically), continuous and intermittent tests are required.

The **continuous relaxation tests** are used to determine the network degradation as function of time and temperature. The procedure is carried out analogously to the classical relaxation test, in which the sample to be examined is brought to a constant strain, and the stress response is recorded. This test is independent from the influence of network reformation as the strain is kept constant for the whole duration while the new network is formed stress-free in the deformed configuration. However, while in the classical relaxation test the stress drop is caused by viscoelastic effects, the stress drop in this long-term experiment is mainly based on chemical degradation of the primary network. In order to determine the influence of the temperature on the degradation process, this experiment is usually performed at different temperature levels. This work also focuses on the influence of the surrounding medium, so that ageing in air and oil is investigated. Special ageing ovens are available in which the experiments can be carried out in parallel. They have several chambers, in which the temperatures and ambient media can be set individually. The samples are placed in these chambers using testing rigs, designed to apply a constant strain. Results of these measurements are shown in Figs. 2 and 3. One can observe a pronounced temperature-dependent decrease in the measured 1st Piola–Kirchhoff stress P_{11}^{-} (so-called engineering stress) in time, which is normalized with its value at the beginning $P_{11,0}$. This decrease can be explained by the network degradation of the NBR. In the final stage of the 100 °C curve, one can observe an increase in force. This increase is supposed to be caused by a shrinkage process, so that after such a long duration at higher temperatures shrinkage of material is not uncommon. Due to the constant length during storage in the testing rig, this results in an increase in effective strain leading to an increase in stress. This is an important side effect of chemical ageing, which was not investigated in this paper. Therefore, the stress signal after the minimum has been neglected.

In order to identify the ageing parameters of the network degradation from Eq. (19), the stress measured over time from the continuous relaxation tests is used and fitted with the approach

$$\begin{aligned} P_{11}^{-} &= P_{11,0}\,(1 - q_\mathrm{d}) \\ q_\mathrm{d} &= \frac{1}{n}\sum_{j=1}^{n} q_\mathrm{d}^{j}, \end{aligned} \tag{21}$$

in which the stress P_{11}^{-} of the degrading network depends on the internal variable q_d in the same sense as the material parameter of this network (Eq. 18). As seen in the experimental data, $P_{11,0}$ cannot be derived directly as the processes of physical relaxation in the beginning of the test and the chemical ageing are overlapping.

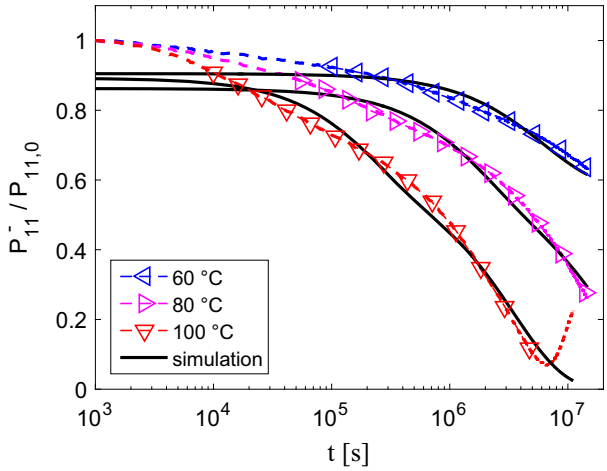

Fig. 2 Continuous relaxation tests and related simulations in air

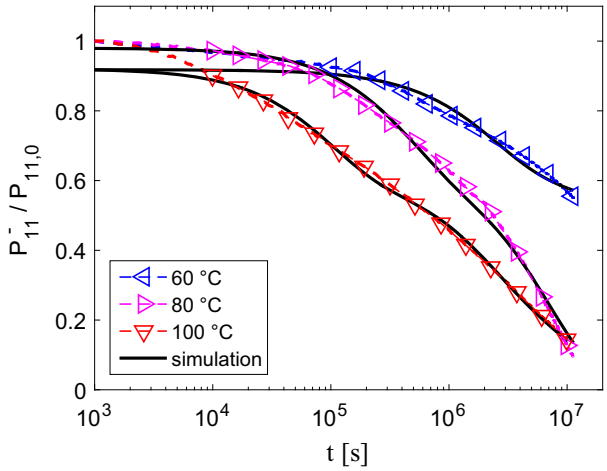

Fig. 3 Continuous relaxation tests and related simulations in oil

Therefore, $P_{11,0}$ is used as a fitting parameter for each curve. In order to introduce more degrees of freedom, a discrete spectrum of ageing variables is used. For the isothermal conditions, Eq. (19) can be solved analytically. This leads to the expressions for the internal variables q_{d}^{j}

$$
\begin{aligned}
q_{\mathrm{d}}^{j} &= 1 - e^{-\frac{t}{\tau_{\mathrm{d}}^{j}(\theta)}} \\
\tau_{\mathrm{d}}^{j}(\theta) &= \nu_{\mathrm{d}}^{j}\, e^{-\frac{E_{\mathrm{d}}^{j}}{R\theta}}.
\end{aligned}
\tag{22}
$$

Since the chemical stress relaxation, resp. the degradation, takes place over several decades, an approach with three evolution equations was used, which corresponds to $n = 3$ in Eq. (21). An approach using three evolution equation was the best option, since using only one or two evolution equations has not led to satisfactory results. The simulations with the identified parameters are shown in Figs. 2 and 3. In these simulations, there is a good agreement between the identified ageing model and the underlying measurements. The experimentally determined relaxation curves are fitted only in the region of the long-term behaviour. The fitting points are represented by triangles, and the viscoelastic short-term behaviour has been omitted.

The **intermittent tests** are carried out in addition to the aforementioned continuous relaxation tests. In these tests, an isothermal load-free ageing of the samples takes place in different ageing media (air, oil). At certain times, ageing is intermitted and the samples are cooled down to room temperature. Relaxation tests or tensile tests can be then carried out with the aged samples at the room temperature, so that a continuation of ageing during this short-time experiment can be excluded. In this work, uniaxial tensile tests with relaxation

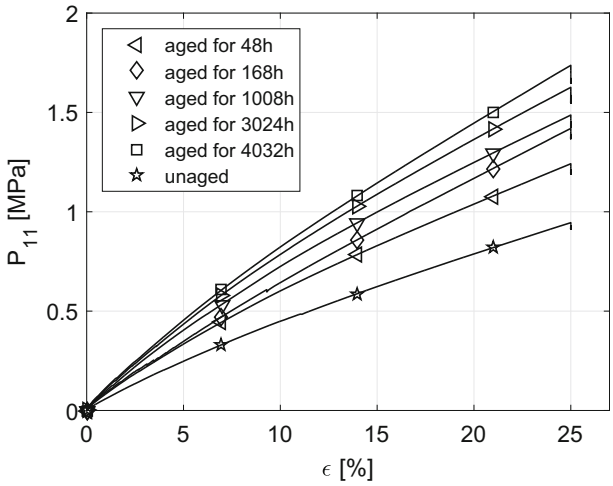

Fig. 4 An example of intermitted tensile tests with NBR samples aged in oil at 80 °C

periods at the end were performed (Fig. 4) with a strain rate of 0.01%/s, such that possible influences of ageing on viscoelasticity were not investigated. It can be seen that the elastomer becomes stiffer as the ageing time increases, which is caused by the reformed network. In the following, an evaluation of the observed tensile curves at certain strains takes place. Combining these data with those from the continuous relaxation tests, so that the contribution of network degradation is subtracted

$$P_{11}^{+}(\lambda_1, t, \theta) = P_{11}(\lambda_1, t, \theta) - P_{11}^{-}(\lambda_1, t, \theta), \tag{23}$$

one obtains the evolution of the stress P_{11}^{+} of the reformed network over the ageing time at certain stretches λ_1 for each ageing temperature θ (Figs. 5, 6). In Eq. (23), the stress P_{11}^{-} of the degrading network can be computed now using the approach (21) with already identified ageing parameters ν_{d}^{j} and E_{d}^{j}. The stress $P_{11,0}(\lambda_1)$ of the unaged material is taken directly from the stress–strain curve of the unaged sample.

In order to identify the ageing parameters of the network reformation ν_{r}^{j} and E_{r}^{j}, the already determined data of the stress P_{11}^{+} are required and fitted with the approach

$$\begin{aligned} P_{11}^{+} &= q_{\mathrm{r}}\, P_{11,\infty} \\ q_{\mathrm{r}} &= \frac{1}{n}\sum_{j=1}^{n} q_{\mathrm{r}}^{j}, \end{aligned} \tag{24}$$

in which P_{11}^{+} depends on the internal variable q_{r} in the same sense as the material tensor of the secondary network (Eq. 33). For a better representation of the experimental data, a spectrum is introduced. For the internal variables of network reformation q_{r}^{j}, a solution is taken similar to Eq. (22). The stress $P_{11,\infty}$ of the fully reformed network ($q_{\mathrm{r}} = 1$) is used as a fitting parameter. Simulations with the identified ageing model of network reformation are shown in Figs. 5 and 6. A good agreement with regard to the experimentally obtained data is visible.

3.2 Material model

Based on the constitutive model presented in Sect. 2, in addition to the ageing parameters the material constants of the rheological model (Fig. 1) have to be identified. A large number of standardized tests can be used for the material investigation (cf. [24] or [7]). In this work, all mechanical measurements are carried out under uniaxial tension. In order to investigate the basic elasticity of the primary network, so-called multi-step relaxation experiments are carried out with the unaged NBR at different temperatures. Hence, the stress–strain curves of the basic elasticity are obtained, which are hardly temperature dependent (see Fig. 7). According to this, the entropy elasticity of rubber is not taken into account. Considering the assumption of

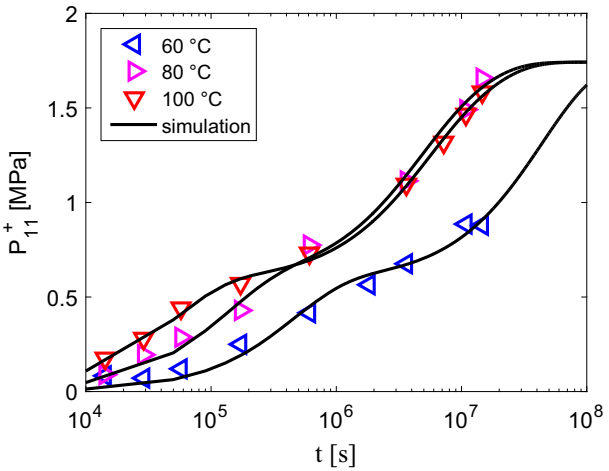

Fig. 5 Stress of the reformed network in NBR samples aged in oil, evaluated at 25% strain

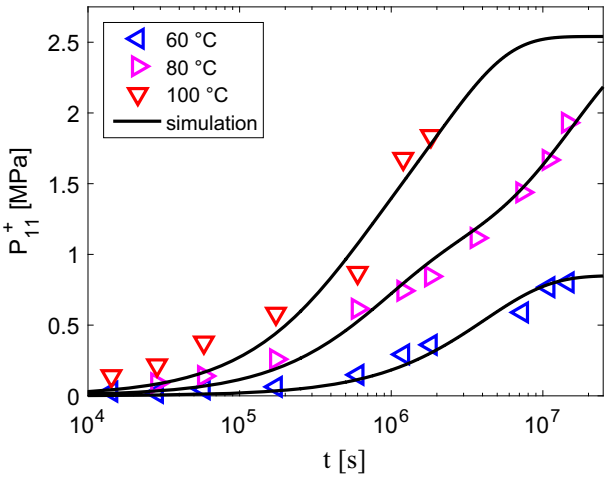

Fig. 6 Stress of the reformed network in NBR samples aged in air, evaluated at 25% strain

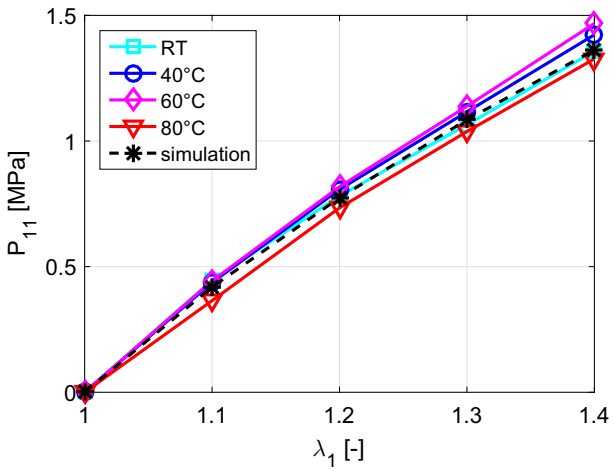

Fig. 7 Stress–strain curves of the basic elasticity at different temperatures and their simulation

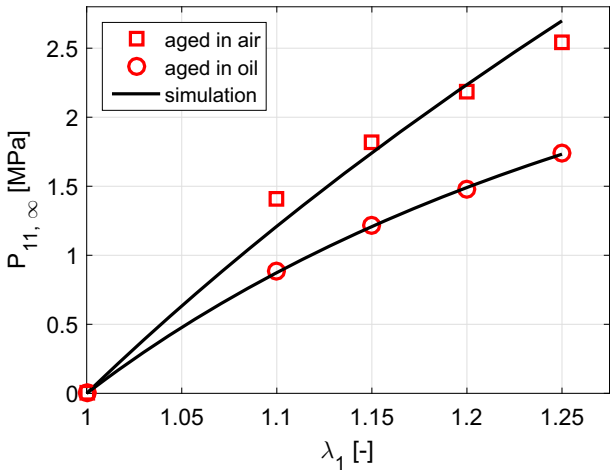

Fig. 8 Stress–strain curves of the reformed network and their simulations

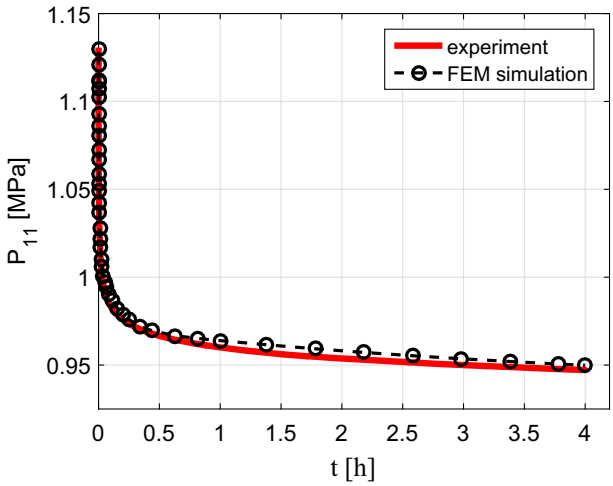

Fig. 9 Relaxation test at room temperature with FEM simulation

mechanical incompressibility, the stress–strain curve can be described with a Neo-Hooke model (Fig. 7), with the corresponding free energy function

$$\rho_0 \, \psi_{\mathrm{d}}(\hat{\mathbf{C}}) = \frac{1}{2} \, \mu_0 \left(I_{\hat{\mathbf{C}}} - 3 \right) . \tag{25}$$

In addition, the relaxation experiments with unaged NBR were carried out (Fig. 9). They are used to characterize the time-dependent material behaviour to be represented by the Maxwell elements. Relaxation experiments were run at room temperature for a period of 4 h. In order to investigate the thermal dependence of the viscosity, these measurements have to be additionally performed at different temperatures. Then, it would be possible to model such a dependence with, for example, the WLF equation (cf. [30]). Such an approach was not considered for this time, because the tension set measurements take place only at room temperature.

Furthermore, it is important to describe the material properties of the secondary network (reformed network). In the previous chapter (Sect. 3.1), only the evolution of the secondary network over ageing time was treated, but its mechanical properties were not investigated. Therefore, with regard to the evaluation of the tensile curves from the intermittent tests at different strains and subsequent parameter identification, a stress–strain relationship for the stress $P_{11,\infty}$ of fully reformed network is obtained (Fig. 8). Assuming mechanically incompressible material behaviour, the Mooney–Rivlin model with the corresponding strain energy density w of the network reformation process is used

$$w = c_{10} \left(I_{\hat{\mathbf{C}}} - 3 \right) + c_{01} \left(I I_{\hat{\mathbf{C}}} - 3 \right) . \tag{26}$$

3.3 Calculation of the model equations

In this part, the general constitutive equations of the model (Eq. 13) are reformulated. This is important for the further numerical implementation. In addition to the already selected material functions (Eqs. 9_3, 16, 25, 26), the Helmholtz free energy function for the volumetric part is chosen according to [27]

$$\begin{aligned}\rho_0\,\psi_{\mathrm{eq}}^{\mathrm{vol}}(J,\theta) = \frac{1}{2}\,K\left[(J-1)^2+(\ln J)^2\right]\\ -K\,\alpha\,(J-1)\,(\theta-\theta_0)-\rho_0\,c(\theta).\end{aligned} \tag{27}$$

A thermo-mechanical term is also introduced here, where α represents the coefficient of volumetric thermal expansion. The function $c(\theta)$ can be determined from calorimetric experiments and is linked to the heat capacity of the material (cf. [15] or [7]), whereby an experimentally motivated approach for $c(\theta)$ was used

$$\frac{\partial^2 c(\theta)}{\partial\,\theta^2} = \frac{A}{\theta}+B. \tag{28}$$

In order to obtain the constitutive equation for the second Piola–Kirchhoff stress tensor $\mathbf{S}$, the Cauchy stress tensor $\mathbf{T}$ is transferred to the reference configuration as follows:

$$\mathbf{S} = J\,\mathbf{F}^{-1}\cdot\left(-p\,\mathbf{I}+\mathbf{T}^{\mathrm{D}}\right)\cdot\mathbf{F}^{-T} = -p\,J\,\mathbf{C}^{-1}+J\,\mathbf{F}^{-1}\cdot\mathbf{T}^{\mathrm{D}}\cdot\mathbf{F}^{-T}. \tag{29}$$

Here, the deviatoric part of Cauchy stress tensor $\mathbf{T}^{\mathrm{D}}$ is defined by Eq. (8). Thus, one can evaluate all partial derivatives of the specific Helmholtz free energy and rewrite Eq. (29), which finally leads to

$$\begin{aligned}
p &= -K\left[(J-1)+\frac{\ln J}{J}\right]+K\,\alpha\,(\theta-\theta_0)\\
s &= \frac{1}{\rho_0}\left(K\,\alpha\,(J-1)+\rho_0\,\frac{\partial c(\theta)}{\partial\theta}\right)\\
\mathbf{S} &= -p\,J\,\mathbf{C}^{-1}+\mu(q_{\mathrm{d}})\,J^{-\frac{2}{3}}\left(\mathbf{I}-\frac{1}{3}\left(\mathrm{tr}\,\hat{\mathbf{C}}\right)\hat{\mathbf{C}}^{-1}\right)\\
&\quad+J^{-\frac{2}{3}}\left(\hat{\mathbf{S}}_{\mathrm{r}}-\frac{1}{3}\left(\hat{\mathbf{S}}_{\mathrm{r}}:\hat{\mathbf{C}}\right)\hat{\mathbf{C}}^{-1}\right)\\
&\quad+\sum_{k=1}^{m}\mu_e^k\,J^{-\frac{2}{3}}\left((\hat{\mathbf{C}}_{\mathrm{i}}^k)^{-1}-\frac{1}{3}\,\mathrm{tr}\left((\hat{\mathbf{C}}_{\mathrm{i}}^k)^{-1}\cdot\hat{\mathbf{C}}\right)\hat{\mathbf{C}}^{-1}\right).
\end{aligned} \tag{30}$$

This constitutive model has a modular structure. Thus, one can see that the stress tensor is additively split into the volumetric part $\mathbf{S}_{\mathrm{vol}}$, the degradative part $\mathbf{S}_{\mathrm{d}}$, the reformative part $\mathbf{S}_{\mathrm{r}}$ and the overstress parts $\mathbf{S}_{\mathrm{neq}}^k$

$$\mathbf{S} = \mathbf{S}_{\mathrm{vol}}+\mathbf{S}_{\mathrm{d}}+\mathbf{S}_{\mathrm{r}}+\mathbf{S}_{\mathrm{neq}}^k. \tag{31}$$

Regarding the reformative part, the integral form of the stress tensor $\hat{\mathbf{S}}_{\mathrm{r}}$ (Eq. 14) is reformulated by using the time differentiation

$$\dot{\hat{\mathbf{S}}}_{\mathrm{r}} = \left[\overset{4}{\mathbf{D}}_{\mathrm{IV}}\,(t)\,q_{\mathrm{r}}(t)\right]:\dot{\hat{\boldsymbol{\Gamma}}} = \frac{1}{2}\left[\overset{4}{\mathbf{D}}_{\mathrm{IV}}\,(t)\,q_{\mathrm{r}}(t)\right]:\dot{\hat{\mathbf{C}}}. \tag{32}$$

The fourth-order material tensor $\overset{4}{\mathbf{D}}$ belongs to the reference configuration and can by defined similar to [12] or [14] as

$$\overset{4}{\mathbf{D}} = 4\,\frac{\partial^2 w}{\partial\mathbf{C}^2}. \tag{33}$$

In order to transform the tensor $\overset{4}{\mathbf{D}}$ to the IVIC, where Eq. (32) is valid, the following transformation rule can be derived

$$\overset{4}{\mathbf{D}}_{\mathrm{IV}} = J^{1/3}\;\overset{4}{\mathbf{D}}. \tag{34}$$

Equation (32) is a hypoelastic formulation in which the rate of the isochoric right Cauchy–Green tensor and the second partial derivative of the strain energy density w (Eq. 26) of the network reformation process read as follows:

$$\begin{aligned}
\dot{\tilde{\mathbf{C}}} &= J^{-\frac{2}{3}} \left(\dot{\mathbf{C}} - \frac{1}{3} \operatorname{tr} \left(\mathbf{C}^{-1} \cdot \dot{\mathbf{C}} \right) \mathbf{C} \right) \\
\frac{\partial^2 w}{\partial \mathbf{C}^2} &= c_{10}\, J^{-\frac{2}{3}} \frac{1}{3} \left[I_{\mathbf{C}} \left(\frac{1}{3} \mathbf{C}^{-1} \otimes \mathbf{C}^{-1} + \left(\mathbf{C}^{-1} \otimes \mathbf{C}^{-1} \right)^{T_{23}} \right) \right. \\
&\quad \left. - \mathbf{C}^{-1} \otimes \mathbf{I} - \mathbf{I} \otimes \mathbf{C}^{-1} \right] \\
&\quad + c_{01}\, J^{-\frac{4}{3}} \frac{2}{3} \left[I I_{\mathbf{C}} \left(\frac{2}{3} \mathbf{C}^{-1} \otimes \mathbf{C}^{-1} + \left(\mathbf{C}^{-1} \otimes \mathbf{C}^{-1} \right)^{T_{23}} \right) \right. \\
&\quad - I_{\mathbf{C}} \left(\mathbf{C}^{-1} \otimes \mathbf{I} + \mathbf{I} \otimes \mathbf{C}^{-1} \right) + \mathbf{C} \otimes \mathbf{C}^{-1} + \mathbf{C}^{-1} \otimes \mathbf{C} \\
&\quad \left. + \frac{3}{2} \left(\mathbf{I} \otimes \mathbf{I} - (\mathbf{I} \otimes \mathbf{I})^{T_{23}} \right) \right].
\end{aligned} \tag{35}$$

4 Results and discussion

The presented constitutive model was implemented in the FE software Comsol Multiphysics using the weak form of the balance of momentum based on the total Lagrangian formulation (cf. [2])

$$\int_{\Omega} \tilde{\mathbf{S}} : \delta \mathbf{E} \, \mathrm{d}\Omega = \int_{\Gamma} \mathbf{t} \cdot \delta \mathbf{u} \, \mathrm{d}\Gamma, \tag{36}$$

whereby the displacement field $\mathbf{u}$ is the primary variable. According to the discretization of the displacement field, a Lagrangian shape function type was used with a quadratic element order. A standard displacement-based method cannot be applied directly, because the shape functions are unable to properly describe the volumetric preserving deformation. In such a case, volumetric locking or numerical instabilities will occur. Therefore, a mixed up finite element formulation is used (cf. [28]). The stress tensor $\mathbf{S}$ is replaced in Eq. (36) by a modified version $\tilde{\mathbf{S}}$

$$\tilde{\mathbf{S}} = \mathbf{S} + (p - \tilde{p})\, J \mathbf{C}^{-1}. \tag{37}$$

In this equation, p is the hydrostatic pressure computed according to Eq. $(30)_1$ and an auxiliary interpolated pressure $\tilde{p}$ is introduced. The interpolated pressure is obtained through an additional weak constraint

$$\int_{\Omega} \left(\frac{\tilde{p}}{K} - \frac{p}{K} \right) \delta \tilde{p} \, \mathrm{d}\Omega = 0, \tag{38}$$

where it is forced to be equal to the hydrostatic pressure p. The order of the shape function for the auxiliary pressure variable should be one order less than that for the displacements.

Similar to the work of [7,15], the balance of internal energy ϵ (cf. [11])

$$\rho_0 \, \dot{\epsilon} = \mathbf{S} : \dot{\mathbf{E}} - \operatorname{Div} \mathbf{Q} + \rho_0 \, r, \tag{39}$$

i.e. the first law of thermodynamics, is considered and evaluated. In the above-mentioned studies, this was taken to compute the thermo-mechanical coupling with respect to dissipative heating. The use here has the consequence of deriving the heat balance in the case of the selected material functions, but without consideration of the dissipative heating. Equation (39) can be reformulated with the help of the Legendre transformation $\epsilon = \psi + \theta \, s$. The calculated stress power and the temporal derivative of the free energy function ψ can be inserted. After neglecting the heat radiation term $\rho_0 \, r$ and the mentioned thermo-mechanical coupling, the heat balance can be finally reformulated as

$$\rho_0 \, \theta \, \dot{s} + \operatorname{Div} \mathbf{Q} = 0. \tag{40}$$

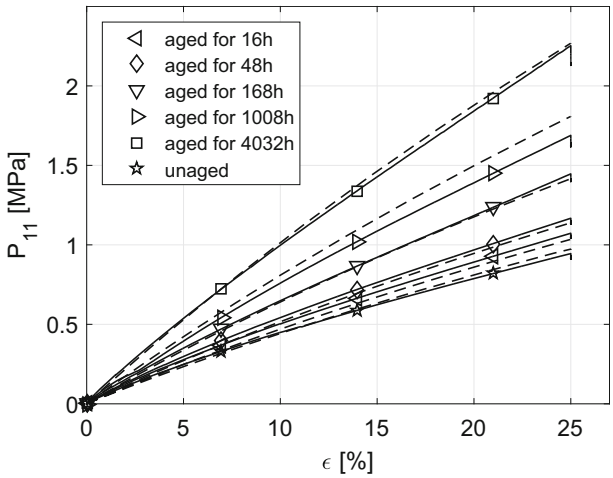

Fig. 10 Tensile tests with samples aged in air at 80 °C. Solid lines describe the measurements, and dashed line describes the FE simulations

In order to solve the temperature-dependent evolution equations (Eqs. 19, 20) not only under isothermal conditions, the heat balance was also implemented using its weak form

$$\int_\Omega \delta\theta \rho_0 \, \theta \, \dot{s} \, \mathrm{d}\Omega + \int_\Omega \mathrm{Grad}(\delta\theta) \, \lambda_\theta \, \mathrm{Grad}(\theta) \, \mathrm{d}\Omega = -\int_\Gamma \delta\theta \, q \, \mathrm{d}\Gamma. \tag{41}$$

It is assumed that all thermo-mechanical properties, measured by using the unaged NBR, are independent on ageing.

The inelastic strain tensor $\hat{\mathbf{C}}_\mathrm{i}^j$, the stress tensor $\hat{\mathbf{S}}_\mathrm{r}$ and the internal variables q_d, q_r are treated as additional degrees of freedom. The shape functions to interpolate all these variables are chosen to be one order lower than those used for the displacements, because these variables add to the strains and stresses computed from displacement derivatives. These variables also do not require continuity between the mesh elements so discontinuous shape functions are used.

First, a validation was carried to check if the implementation works correct and is performed on relaxation time simulation in uniaxial tension mode at room temperature. The result is shown in Fig. 9. One can see a very good match with the underlying experiment over the whole time period. This shows that the implementation works well, and in the next step we are oriented to the simulation of tensile tests and tension set.

Now, the tensile tests with aged NBR specimens are simulated and compared with the measurements. First, a load-free isothermal ageing of the specimens is simulated in different media (air, oil). Then, uniaxial tensile tests at room temperature are simulated on the aged specimens (see Figs. 10, 11, 12, 13). The strain rate corresponds to 0.01%/s. This validation shows that the model can represent the mechanical and the ageing behaviour well. Thus, the ageing-induced stiffening of the material can be simulated in a good way with respect to different ageing media. For some curves (e.g. 168 h at 100 °C in air), the quality of the simulation still leaves some room for improvement. However, such deviations can also be influenced by the inaccuracies in the parameter identification or experimental scattering.

The tension set measurements are often used in sealing production and design. In this work, the tension set measurements were carried out according to the german norm DIN ISO 2258 and also used to validate the presented modelling of ageing. For this purpose, tensile specimens are stored under specified deformation at a certain temperature in the ageing medium (air, oil) and are then taken out after certain ageing times after which they are released. The elastomer samples then begin to return (relax) to their equilibrium shape. However, this has changed due to the ageing (network degradation and reformation) occurring during storage. This is shown by the fact that the sample length L_0, which was determined before storage, is no longer reached. After the interruption of ageing and unloading the sample, the aged length L_age is measured after certain time periods and the tension set (TS) can be calculated

$$\mathrm{TS} = 100 \cdot \frac{L_\mathrm{age} - L_0}{L - L_0}. \tag{42}$$

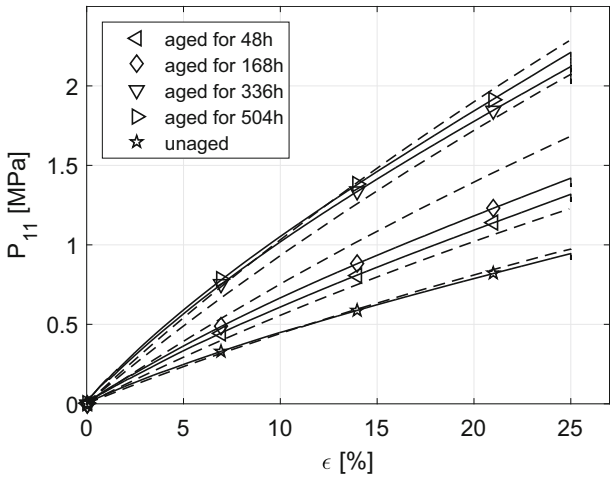

Fig. 11 Tensile tests with samples aged in air at 100 °C. Solid lines describe the measurements, and dashed line describes the FE simulations

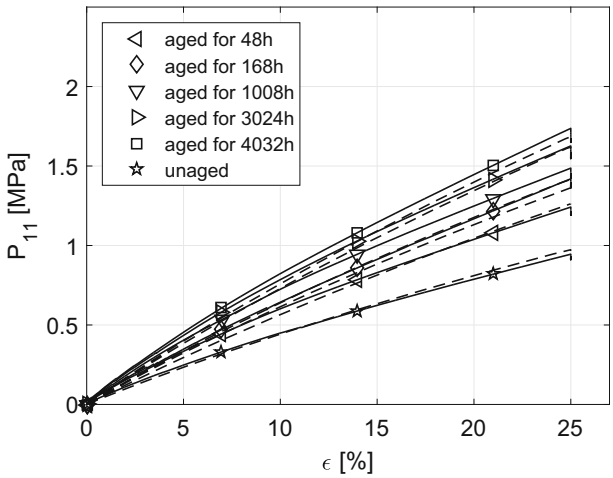

Fig. 12 Tensile tests with samples aged in oil at 80 °C. Solid lines describe the measurements, and dashed line describes the FE simulations

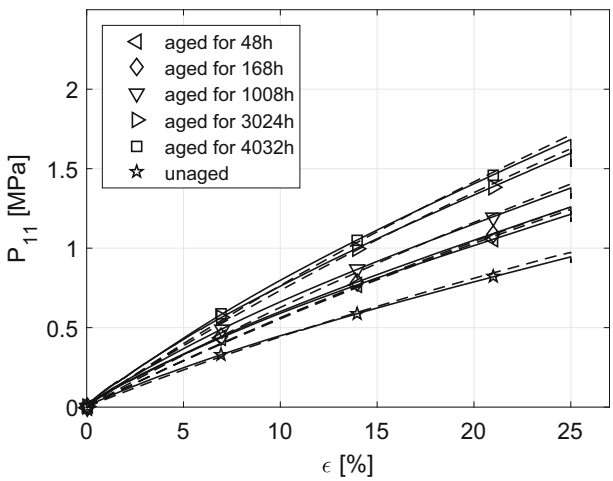

Fig. 13 Tensile tests with samples aged in oil at 100 °C. Solid lines describe the measurements, and dashed line describes the FE simulations

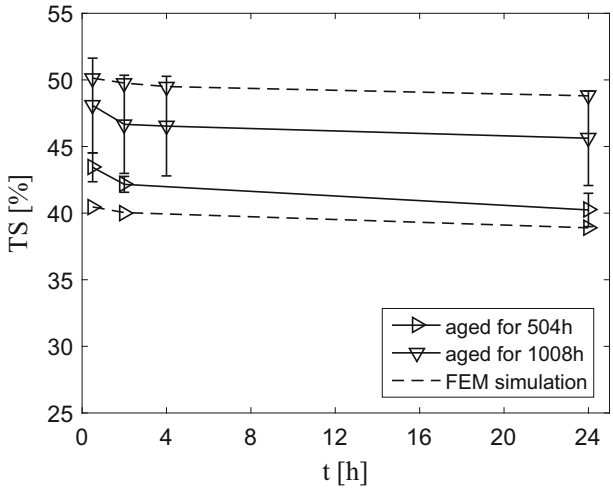

Fig. 14 Tension set measurements on samples aged in air at 80 °C and their FEM simulations

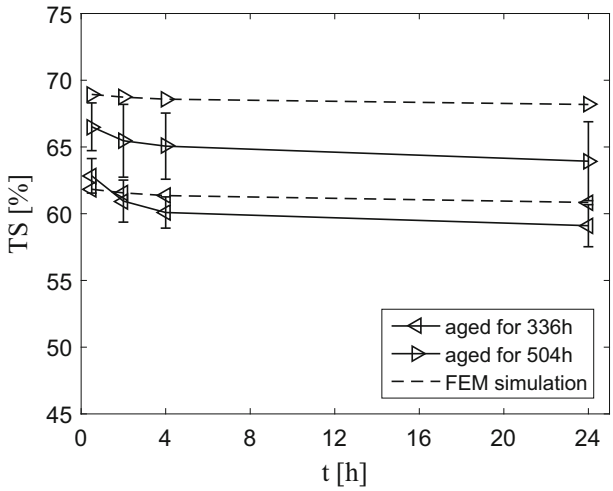

Fig. 15 Tension set measurements on samples aged in air at 100 °C and their FEM simulations

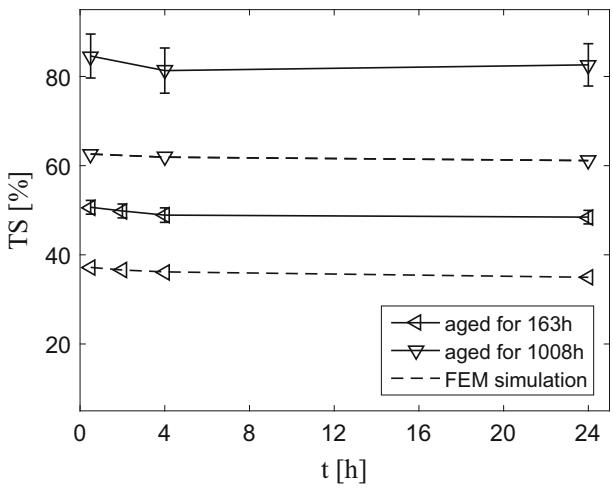

Fig. 16 Tension set measurements on samples aged in oil at 100 °C and their FEM simulations

Table 2 List of material and ageing parameters

Parameter	Medium	Value	Unit
μ_0	–	1.5315×10^6	[Pa]
μ_e^1	–	0.0780×10^6	[Pa]
μ_e^2	–	0.1113×10^6	[Pa]
μ_e^3	–	0.0679×10^6	[Pa]
μ_e^4	–	0.0624×10^6	[Pa]
r^1	–	4.2133	[s]
r^2	–	60.391	[s]
r^3	–	9.6483×10^2	[s]
r^4	–	3.8439×10^4	[s]
c_{10}	Air	2.2080×10^6	[Pa]
c_{01}	Air	4.3264×10^3	[Pa]
E_d^1	Air	1.1433×10^5	[J/mol]
E_d^2	Air	1.0049×10^5	[J/mol]
E_d^3	Air	1.0049×10^5	[J/mol]
ν_d^1	Air	4.8344×10^{10}	[1/s]
ν_d^2	Air	3.3678×10^7	[1/s]
ν_d^3	Air	3.3679×10^7	[1/s]
E_r^1	Air	3.9271×10^4	[J/mol]
E_r^2	Air	1.0733×10^5	[J/mol]
E_r^3	Air	1.0738×10^5	[J/mol]
ν_r^1	Air	0.8496	[1/s]
ν_r^2	Air	4.6811×10^8	[1/s]
ν_r^3	Air	4.7673×10^8	[1/s]
c_{10}	Oil	1.1470×10^5	[Pa]
c_{01}	Oil	1.6316×10^6	[Pa]
E_d^1	Oil	8.3643×10^4	[J/mol]
E_d^2	Oil	1.1264×10^5	[J/mol]
E_d^3	Oil	6.4873×10^4	[J/mol]
ν_d^1	Oil	5.4098×10^6	[1/s]
ν_d^2	Oil	2.9423×10^9	[1/s]
ν_d^3	Oil	95.302	[1/s]
E_r^1	Oil	5.6733×10^4	[J/mol]
E_r^2	Oil	6.2794×10^4	[J/mol]
E_r^3	Oil	3.4384×10^4	[J/mol]
ν_r^1	Oil	1.7732×10^3	[1/s]
ν_r^2	Oil	1.5874×10^2	[1/s]
ν_r^3	Oil	0.0056	[1/s]
ρ_0	–	1.18×10^3	[kg/m^3]
A	–	716	[J/kg K]
B	–	2.36	[J/kg K^2]
λ_θ	($\theta = 293$K)	0.3374	[W/m K]

Here, L is the stretched length of the sample during storage. If the material is unaged or unaffected by the ageing medium, the TS is equal to zero. If the length L remains constant after unloading the sample, then is the TS equal to 100%.

In the same way, the tension set procedure was simulated with the proposed constitutive model using FEM. The results for different ageing media and temperatures are shown in Figs. 14, 15 and 16. With regard to ageing in air (Figs. 14, 15), one can observe a good agreement between the simulations and the underlying tension set measurements. However, it can be seen that the measured TS shows a more pronounced relaxation compared to the simulation, which results in some qualitative deviation. This can be further improved by investigating and modelling the possible effects of ageing on viscoelasticity. However, in general one can conclude that the model can represent the tension set behaviour well.

In case of ageing in oil (Fig. 16), a significant larger deviation between the measured tension and simulated tension set can be seen. After storage of the samples in oil, we have detected a swelling phenomenon that distorts the results. Therefore, the measured data from the tension set lead to higher values. The constitutive model does not consider swelling; therefore, these results cannot be assessed. However, an option to validate modelling of ageing in oil using tension set would be possible with the use of non-swelling oils, or taking

the NBR with a higher content of acrylonitrile. Otherwise, swelling phenomena has to be considered in the proposed constitutive model.

5 Conclusion

In this work, the modelling of the homogeneous ageing of nitrile rubber was studied with regard to its viscoelasticity. The proposed continuum mechanical model was based mainly on the works of [13–15,21]. Experimental investigations of aged or unaged NBR and a subsequent parameter identification was carried out. A total of 41 material parameters were determined on the basis of investigations carried out in different ageing media (see Table 2). In general, the simulations with the identified models show a good agreement with the underlying experiments. Subsequently, the proposed constitutive model was implemented in a commercial FE software and validated by means of tensile tests with variously aged NBR specimens and tension set measurements. Here, the capability of the model to simulate this complex material behaviour was shown and some possible improvements have been discussed. In the case of industrial applications, this model can be used to simulate the ageing of NBR taking viscoelasticity into account and thus, for example, to depict the tension or compression set behaviour in time, which is necessary for lifetime predictions of rubber components.

In this paper, ageing was regarded as an homogeneous process. However, in many industrial applications, components of larger dimensions are used so that diffusion-limited oxidation (DLO) needs to be considered. DLO can occur whenever the rate of oxygen consumption within the material is greater than the rate at which it can be resupplied by diffusion from the surrounding medium. This can lead to a heterogeneously oxidized material [10]. For these reasons, it would be of great importance to consider inhomogeneities, diffusivity and reactivity of the medium and elastomer in the modelling of ageing, as, for example, proposed in the work of [16].

Acknowledgements The financial support of the project by the Deutsche Forschungsgemeinschaft (DFG) under the Grant Number JO 818/3-1 is gratefully acknowledged.

References

1. Andrews, R., Tobolsky, A., Hanson, E.: The theory of permanent set at elevated temperatures in natural and synthetic rubber vulcanizates. J. Appl. Phys. **17**, 352–361 (1946)
2. Bathe, K.J.: Finite Elemente Procedures, 2nd edn. Prentice-Hall, Englewood Cliffs (1996)
3. Blum, G., Shelton, J., Winn, H.: Rubber oxidation and ageing studies. Ind. Eng. Chem. **43**, 464–471 (1951)
4. Budrugeac, P., Segal, E., Ciutacu, S.: Thermooxidative degradation of nitrile-butadiene rubber. J. Therm. Anal. **37**, 1179–1191 (1991)
5. Celina, M., Wise, J., Ottesen, D., Gillen, K., Clough, R.: Oxidation profiles of thermally aged nitrile rubber. Polym Degrad Stab **60**, 493–504 (1998)
6. Coleman, B.D., Noll, W.: The thermodynamics of elastic materials with heat conduction and viscosity. Arch. Ration. Mech. Anal. **13**, 167–178 (1963)
7. Dippel, B.: Experimentelle Charakterisierung, Modellierung und FE-Berechnung thermomechanischer Kopplungen am Beispiel eines rußgefüllten Naturkautschuks. Ph.D. thesis, Universität der Bundeswehr München (2015)
8. Ehrenstein, G., Pongratz, S.: Beständigkeit von Kunststoffen. Carl Hanser Verlag, Munich (2007)
9. Flory, P.J.: Thermodynamic relations for hight elastic materials. Trans. Faraday Soc. **57**, 829–838 (1961)
10. Gillen, K.T., Clough, R.L., Wise, J.: Prediction of Elastomer Lifetimes from Accelerated Thermal-Aging Experiments. ACS Publications, Washington (1996)
11. Haupt, P.: Continuum Mechanics and Theory of Materials. Springer, Berlin (2000)
12. Hossain, M., Possart, G., Steinmann, P.: A finite strain framework for the simulation of polymer curing. Part I: elasticity. Comput. Mech. **44**, 621–630 (2009)
13. Johlitz, M.: On the representation of ageing phenomena. J. Adhes **88**, 620–648 (2012)
14. Johlitz, M., Diercks, N., Lion, A.: Thermo-oxidative aging of elastomers: a modelling approach based on a finite strain theory. Int. J. Plast. **63**, 138–151 (2014)
15. Johlitz, M., Dippel, B., Lion, A.: Dissipative heating of elastomers: a new modelling approach based on finite and coupled thermomechanics. Contin. Mech. Thermodyn. **28**, 1111–1125 (2016)
16. Johlitz, M., Lion, A.: Chemo-thermomechanical ageing of elastomers based on multiphase continuum mechanics. Contin. Mech. Thermodyn. **25**, 605–624 (2012). https://doi.org/10.1007/s00161-012-0255-8
17. Johlitz, M., Retka, J., Lion, A.: Chemical ageing of elastomers: experiments and modelling. In: Jerrams, S., Murphy, N. (eds.) Constitutive Models for Rubber, vol. VII, pp. 113–118. Taylor & Francis, Boca Raton (2011)
18. Lee, E.H.: Elastic–plastic deformation at finite strain. J. Appl. Mech. **36**, 1–6 (1969)
19. Lion, A.: Thermomechanik von Elastomeren. Berichte des Instituts für Mechanik der Universität Kassel (Bericht 1/2000) (2000)

20. Lion, A., Dippel, B., Liebl, C.: Thermomechanical material modelling based on a hybrid free energy density depending on pressure, isochoric deformation and temperature. Int. J. Solids Struct. **51**, 729–739 (2014)
21. Lion, A., Johlitz, M.: On the representation of chemical ageing of rubber in continuum mechanics. Int. J. Solids Struct. **49**, 1227–1240 (2012)
22. Lubliner, J.: A model of rubber viscoelasticity. Mech. Res. Commun. **12**, 93–99 (1985)
23. Santoso, M., Torrejon, Y.N., Giese, U., Schuster, R.H.: Untersuchung thermischer und oxidativer alterungsprozesse von elastomeren; verbrauch von p-phenylendiaminen mit der chemilumineszenz. Kaut. Gummi Kunstst. **61**, 306–311 (2008)
24. Scheffer, T., Seibert, H., Diebels, S.: Optimisation of a pretreatment method to reach the basic elasticity of filled rubber materials. Arch. Appl. Mech. **83**, 1659–1678 (2013)
25. Sedlan, K.: Viskoelastisches Materialverhalten von Elastomerwerkstoffen, Experimentelle Untersuchung und Modellbildung. Dissertation, Berichte des Instituts für Mechanik (2/2001), Universität Gesamthochschule Kassel (2001)
26. Shaw, J., Jones, S., Wineman, A.: Chemorheological response of elastomers at elevated temperatures: experiments and simulations. J. Mech. Phys. Solids **53**, 2758–2793 (2005)
27. Simo, J.C., Taylor, R.L.: Penalty function formulations for incompressible nonlinear elastostatics. Comput. Methods Appl. Mech. Eng. **35**, 107–118 (1982)
28. Sussman, T., Bathe, K.J.: A finite element formulation for nonlinear incompressible elastic and inelastic analysis. Comput. Struct. **26**, 357–409 (1987)
29. Tobolsky, A.V.: Mechanische Eigenschaften und Struktur von Polymeren. Berliner Union, Stuttgart (1967)
30. Williams, M.L., Landel, R.F., Ferry, J.D.: The temperature dependence of relaxation mechanisms in amorphous polymers and other glass-forming liquids. J. Am. Chem. Soc. **77**, 3701–3707 (1955)
31. Wise, J., Gillen, K., Clough, R.: An ultrasensitive technique for testing the Arrhenius extrapolation assumption for thermally aged elastomers. Polym. Degrad. Stab. **49**, 403–418 (1995)